Thermal and hydrothermal ageing of flax/polypropylene composites and their stainless steel hybrid laminates

Jérôme Rousseau, Noelle Edwige Ngoufo Donkeng, Fabienne Farcas, Sébastien Chevalier, Vincent Placet

Thermal and hydrothermal ageing of flax/polypropylene composites and their stainless steel hybrid laminates

Jérôme Rousseau[1*], Noëlle-Edwige Ngoufo Donkeng[1,2,3], Fabienne Farcas[4], Sébastien Chevalier[3], Vincent Placet[2]

[1]DRIVE Lab, Université Bourgogne, Nevers, France

[2] FEMTO-ST Institute, Department of Applied Mechanics, Université Franche-Comté, F-25000 Besançon

[3] ICB UMR 6303 CNRS, Université Bourgogne, F-21000 Dijon

[4] CPDM, Université Gustave Eiffel, F-77454 Marne-la-Vallée

*corresponding author: jerome.rousseau@u-bourgogne.fr

Abstract:

Due to their numerous advantages, such as light weight, sustainability, cost and damping capacity, plant fibre composites (PFCs) have been recently introduced into fibre metal laminates (FMLs). The present study is focused on the thermal and hydrothermal ageing of flax/polypropylene composites and their stainless steel hybrid laminates. The results show that hybridization of PFCs with thin stainless steel sheets provides a significant increase in bending and impact properties. Immersion in water at 70 °C induces a significant decrease in bending properties, but the bending stiffness of the laminates is still suitable for semi-structural applications. No significant influence on the impact force and energy absorption but a change in the deformation mode are observed for the considered ageing times. Thermal ageing in air at 120 °C induces a significant degradation in the bending and impact properties of the composites for

exposure times longer than 50 days. This is mainly due to the embrittlement of the polypropylene induced by thermal oxidation.

Keywords: A. Biocomposite, B. Environmental degradation, Impact behaviour, D. Mechanical testing

Introduction

Hybridization, a proven strategy to toughen composites, involves the combination of two or more types of materials or fibres. Fibre metal laminates are a good approach to overcome most limitations of metal and polymeric composites. They belong to a subfamily in which thin metal layers alternate with composite plies. When compared to single-component materials, FMLs provide added functionalities such as high bending strength, fatigue and impact resistance, damage tolerance, acoustic absorption, vibration transmissibility and damping characteristics [1-3]. They have been applied in the transportation sector for decades [4-6]. FMLs with a sandwich structure have also been developed more recently for use in the construction sector. They are made of two external skins thermally bonded to a polymeric core and are referred to by the SCM acronym, which stands for Steel Composite Materials. They are used as tough materials with good energy absorption, high durability, impact resistance and aesthetic advantages. The introduction of such materials in the manufacturing of lightweight portable outdoor structures, such as urban furniture, represents an interesting opportunity.

When reviewing the history of FML developments, a strong evolution in material selection can be seen. After a first generation made of aluminium and fibre reinforced

thermoset resin composites, including the most widely known examples of GLARE (glass laminate aluminium reinforced epoxy), CARALL (carbon aluminium laminate) and ARALL (aramid aluminium laminate), the second generation was characterized by the utilization of thermoplastic matrices for the composite parts, which provide shorter manufacturing cycles, reduced cost and greater flexibility in manufacturing process, recycling and repair, and more versatility in attainable shapes [7]. Recently, increasing environmental concerns have encouraged researchers to develop new ranges of sustainable FMLs made of wood and plant fibre composites [3, 8-12]. In order to maintain consistency with the naming conventions of previous solutions, new acronyms have been introduced, such as SIRAL (sisal fibre reinforced aluminium laminates) [3] and CAJRALL (carbon-jute reinforced aluminium laminate) [12]. Plant fibre composites have many advantages related to light weight, cost, mechanical performance, and damping capacity [13, 14], and they are good candidates to reduce the carbon footprint of composite materials and associated FMLs. For example, the life cycle of wood-aluminium laminated (WAL) panels was recently assessed [11]. The results showed that the environmental impact of manufacturing was less for WAL panels than aluminium honeycomb panels. Wood-based composite manufacturing showed environmental advantages in all damage categories except in ecosystem quality, while aluminium alloy sheet manufacturing played an important role in the environmental impact for laminated panel development [11].

While the main advantages of this most recent generation of FMLs made of biobased composites are quite well illustrated in the recent literature, it remains necessary to investigate their long-term durability. Indeed, plant and wood fibres are very sensitive to hygrothermal and hydrothermal conditions, and the durability of PFCs is still an open

question [15]. The adhesion between the metal and the PFC layers in the frames of FMLs, already identified as a critical constraint [9-11], requires specific attention and investigation under various ageing conditions.

This paper studied steel composite materials prepared from flax polypropylene and their hybrids obtained by the addition of stainless steel external skins. Their service properties for outdoor use involve variable environmental conditions, among which humidity and temperature were selected for the present study. To investigate the effects of ageing, the samples were forced to undergo oxidative degradation. Therefore, severe conditions were applied, i.e., water immersion at 70 °C and heating at 120 °C. The effects of these two accelerated ageing conditions were studied through visual examination, mass and dimension evolutions, molecular characteristics using spectroscopic analysis, and mechanical properties selected for their ability to represent the intended use (3 point bending and impact).

Materials and methods

Materials

The two materials selected for the preparation of the composites and hybrid specimens were a flax/polypropylene composite and stainless steel. The composite material used in this study was Nattex (Dehondt Composites, Port-Jérôme-sur-Seine, France) constituted from a 3/1 twill fabric pre-impregnated with a polypropylene matrix (60% mass fraction, areal weight 800 g/m²). Figure 1 presents the elementary cell of the fabric. The elastic properties of the composite material are presented in Table 1. E_1 and E_2 are the weft and warp moduli, respectively, ν_{12} is Poisson's ratio and G_{12} is the shear modulus of the composite. These properties were measured by a tensile test at a rate of 2 mm/min

at room temperature using an universal tensile testing machine MTS Criterion C45 (MTS, Eden Prairie, USA). The shear modulus G_{13} was measured by means of a short beam shear test. The skins were made of austenitic stainless steel K41X (Aperam, Isbergues, France). Its mechanical properties, measured by a tensile test for E and ν, and calculated from these values for G, are also listed in Table 1.

Manufacturing

Composite plates were made from only Nattex to study the ageing behaviour of the flax/PP material. The specimens were produced using non-dry materials. As evidenced by recent research, the utilization of non-dry flax fibers in processing can improve the mechanical performances and durability of composites, particularly when utilizing matrices that are less sensitive to moisture [16-18]. The Nattex material was stored in a room in which the temperature was measured between 19 and 21°C and the relative humidity between 30 and 40%. The moisture content of the material was at equilibrium under these hygrothermal conditions. Four plies were stacked with a sequence $[90/0]_2$. The laminate was manufactured in a Fontijne TPC 321 thermocompression press (Fontijne Presses, Delft, The Netherlands). The temperature cycle included a temperature increase at a rate of 5 °C/min to 170 °C, followed by a 5-min plateau, then cooling of the laminate at 5 °C/min to room temperature. A pressure of 3 bars was applied at the beginning of the plateau and maintained until the end of the cycle. Samples made exclusively from polypropylene were also produced using the side regions of Nattex plies containing no fibers. The material was melted and shaped into sheets using the same temperature cycle employed in the manufacture of composite plates.

Hybrid specimens with the same dimensions (350 mm x 350 mm) were manufactured using the same temperature/pressure cycle. The only difference was that two steel skins (0.2 mm thick) were bonded to the composite with a thermoplastic ethylene/vinyl acetate copolymer adhesive film Pontacol 20.201 (Everad Adhesives, Marlenheim, France). The metal sheets were abraded with sandpaper and degreased with acetone before bonding.

The final average thickness of the plates was 3.4 mm for the composite alone and 3.8 mm for the hybrid plates. Composite and hybrid samples were cut using a ProtoMAX water jet cutting machine (Omax, Washington, USA). The dimensions of the samples were 170 mm x 25 mm for the three-point bending tests and 100 mm x 100 mm for the impact tests. The specimens were conditioned at 23 °C and 50% RH for 7 days before the initial tests.

Ageing methods

Two ageing methods were selected for this study. For hydrothermal ageing, samples were immersed in distilled water at 70 °C. For thermal ageing, samples were placed in an oven at 120 °C. In both cases, the samples were periodically removed for dimensional measurements and weighed using an electronic balance Radwag PS 1000.R1 with 0.001 g precision (Radwag, Radom, Poland). The specimen edges were not protected to allow water absorption even in the presence of the stainless steel skins. The aged specimens used for mechanical characterization were removed from the water or the oven and placed in airtight sealed bags before testing, which was performed within 24 hours.

IR spectroscopy

Infrared spectra were obtained using a Nicolet iS20 (Thermo Fisher Scientific, Waltham, MA USA) equipped with an ID7-ATR spectrometer with a diamond crystal with a fixed incident angle of 45°. The specimens were analysed in triplicate by absorbance spectra in the region between 4000 and 400 cm^{-1} with 32 scans at 4 cm^{-1} resolution using OMNIC 9 software provided by ThermoFisher Scientific.

To monitor the ageing process of flax/polypropylene composite, the changes in the obtained spectra were analysed. Significant focus was given to two specific characteristic bands. The first, centred at approximately 1730 cm^{-1}, is associated with the carbonyl function (C=O) and is linked to the presence of stabilizers and to the oxidation of the polypropylene [19]. The second characteristic band, centred at approximately 1640 cm^{-1}, is related to the conjugated carbonyl group and is representative of lignin [20]. In order to eliminate the influence of variations in the IR beam penetration depth on the analysed quantities and given that the amount of alkyl groups remains relatively constant during ageing, the monitoring was carried out using the structural indices determined by the equations below:

$$I_{C=O} = \left(\frac{\text{Area of carbonyl band centered around } 1730\ cm^{-1}}{\text{Area of alkyl band between } 3060 cm^{-1} \text{ and } 2760 cm^{-1}}\right) \times 100 \quad (1)$$

$$I_{lignin} = \left(\frac{\text{Area of carboxyle of lignin band centered around } 1640\ cm^{-1}}{\text{Area of alkyl band between } 3060 cm^{-1} \text{ and } 2760 cm^{-1}}\right) \times 100 \quad (2)$$

Scanning Electron Microscopy

A JEOL JSM-7600F SEM (Jeol, Tokyo, Japan) was utilized to investigate the surface morphology and ageing effects of specimens at a magnification ranging from x25 to x65, with a 5 kV accelerating voltage. The samples were coated with gold before analysis.

Mechanical testing

Bending test

Three-point bending tests were performed using the MTS C45 tensile testing machine, according to the ISO 14125 standard. The dimensions of the tested specimens were 170 mm in length and 25 mm in width. A span of 100 mm and a deflection rate of 2 mm/min were used for all the tests. The bending modulus, strength and strain at failure were then determined according to the standard.

Impact testing

Impact tests were performed on a Dynatup 9250 instrumented drop tower (Instron, Norwood, USA). The square specimens, 100 x 100 mm, were clamped by a pneumatic fixture, leaving a 76 mm diameter circular unclamped opening. The tup had a hemispherical head with a diameter of 20 mm. The falling mass had a weight of 5.88 kg, and the falling height was fixed at 0.35 m to obtain an impact energy of 20 J for all specimens. This impact energy was selected after conducting initial tests that demonstrated its ability to puncture unaged specimens. Data recorded by the machine were the impactor initial velocity and the impact load at a frequency of 410 kHz. Other values, such as impactor velocity, displacement, and energy evolution, were derived from the load and time data. Absorbed energies were calculated by integration of the complete load displacement curve for hybrid samples (with impactor rebound), whereas for composite samples, where perforation occurred, only the part of the curve until the maximum load was considered for this integration.

Mechanical tests after hydrothermal ageing were performed on the water-saturated specimens and at ambient temperature. In the case of thermal ageing, mechanical tests were performed on the dried material at ambient temperature.

Single-lap shear test

Single-lap specimens were used to evaluate the adhesion between the composite and the stainless steel. The single-lap joints were manufactured using a composite plate and a 2 mm thick steel plate of the same grade as the skins. The 300 x 150 mm plates were stacked with a 25 mm overlap length and assembled in the thermocompression press using the same procedure as for the hybrids. The assembly was then cut with a water jet into 25 mm wide specimens. Tensile tests were performed using the MTS C45 tensile testing machine equipped with offset jaws at room temperature and at 100 °C. Adhesion was characterized by the shear strength of the lap joints.

Results

Hydrothermal ageing

The evolution of the mass of the composite and hybrid specimens as a function of the immersion time in distilled water at 70 °C is presented in Figure 2.

For the composite, the evolution was similar for the bending and impact specimens, which had dissimilar geometries. After rapid water uptake during the first ten days, stabilization at approximately 8% weight gain was observed between ten and forty days. This significant water uptake was mainly due to the hydrophilicity of the flax fibres. The order of magnitude was consistent with that of previous studies [21, 22]. Water uptake resulted from both the diffusion of water in the composite through the main plate

faces and capillary mechanisms originating from the unprotected edges. A progressive and quasi-linear mass loss was then observed from 40 to 180 days of ageing. This mass loss was attributed to the degradation and leaching of the flax fibres. Immersion in hot water is well known to induce the extraction and hydrolysis of pectins and hemicelluloses from flax and then their release and dissolution in water [23]. These biochemical modifications could also explain the significant change in colour observed during hydrothermal ageing (Figure 3). It was observed a colour change from yellow–brown before flax was immersed to dark-grey when it was immersed and water-saturated. Similar colour transitions were previously observed for flax and hemp fibres during dew retting [24, 25]. This darkening in the fibres was attributed to the metabolic activities of microorganisms during retting [26]. After hydrothermal ageing and drying, the fibres returned to a clear and whitish colour (Figure 3c).

When stainless steel skins were added to the composite, the sorption kinetics slowed, particularly for the square specimens (prepared for impact tests). Almost 50 days were necessary to reach equilibrium. In this case, water sorption was only possible through the specimen edges. Interestingly, with the hybrid material, equilibrium was then maintained during ageing. A slight onset in mass loss was observed after 140 days of ageing. The skins constituted protective layers that impeded the leaching of the composite and the release of hydrolysed material.

Hydrothermal ageing also induced changes in the PP matrix, as revealed by FTIR (Figure 4). For composites immersed in water, the region of the FTIR spectrum between 1500 cm^{-1} and 1800 cm^{-1} showed a decrease in the carbonyl band at 1730 cm^{-1} over time and an increase in a large band at approximately 1640 cm^{-1}.

The absorption band at 1730 cm^{-1} was characteristic of carbonylated stabilizers PP. Thus, this decrease showed that these components were extracted in the aqueous environment [27]. This phenomenon, highlighted by the evolution of $I_{C=O}$ in Figure 5a, appeared to be rapid from the time of immersion to 50 days, and a slower decrease was observed up to 177 days. Additionally, the increase in the absorption at approximately 1640 cm^{-1}, which was related to lignin, revealed loss of polymer at the surface of the composite and therefore exposure of the flax fibres. Again, the phenomenon started after 30 days and became significant at 177 days, as shown by the evolution of I_{lignin} in Figure 5b.
Hydrothermal ageing also induced a significant effect on the bending properties of the composite and hybrid materials (Figure 6 and Figure 7). For composites alone, a significant decrease in the bending modulus was observed from the earliest ageing days (Figures 6a and 7a). It dropped from approximately 8 GPa to 1.9 GPa after ten days and then remained constant during ageing. A slight increase was observed for the last measured time (177 days). This general decrease in stiffness was mainly attributed to a reversible mechanism, the plasticization of the flax fibres by water. This was consistent with the significant increase in the strain at failure (Figure 7c). The loss of stiffness was attributed in part to damage. Indeed, the swelling of the fibres induced by water absorption in their wall also generated stresses that may have caused cracking and delamination at the fibre/matrix interface [28-30]. Such damage could explain the significant decrease in bending strength (Figure 7b).

For the hybrid material, hydrothermal ageing also induced a significant decrease in the bending properties (Figures 6b, 7d, 7e and 7f). For the composite, the bending properties initially dropped and then remained substantially stable during ageing. Decreases of approximately 55%, 65% and 70% were measured for the bending

modulus (Figure 7d), strength (Figure 7e) and strain at failure (Figure 7f), respectively. This was attributed to softening and degradation of the composite but also to degradation at the interfaces between the composite and the stainless steel skins. Cohesive failure was observed in the buckling zone of the flexural beams tested before ageing (Figures 8a and 8b), which highlighted the good efficiency of the adhesive film. A more complex failure mode was observed after 30 days of hydrothermal ageing (Figure 8c and 8d) that combined buckling and delamination at the adhesive film (caption 1 in Figure 8e) but also cohesive failure in the composite (caption 2 in Figure 8e).

The significant effect of hybridization also deserves to be emphasized. Before ageing, the bending stiffness and strength were 6 and 3 times larger for hybrid than for composite specimens, respectively (Figure 7). After 177 days of hydrothermal ageing, the remaining bending stiffness and strength in the water-saturated state were approximately 20 GPa and 70 MPa, respectively, a performance that was still suitable with respect to most of the requirements for semi-structural applications.

The impact behaviour was also significantly affected by hydrothermal ageing for both composites and hybrids. In the case of composite specimens (Figure 9a), the initial slope of the load displacement curve decreased after 10 days of ageing and remained stable thereafter. This was consistent with the modulus drop observed in bending specimens. The maximum load slightly increased in the first period of ageing and strongly reduced after 177 days (Table 2). Observations of the impacted specimens showed that the perforation induced marked orthogonal cracks along the fibre directions in unaged specimens (Figure 10a). For specimens aged 10, 30 and 50 days, the damage was more diffuse in the affected area. At 177 days, the cracks were again very marked,

but the affected area was strongly reduced in size compared to the unaged specimens. This behaviour could have been related to evolution of the plasticity of the material, which would have been consistent with the evolution of the failure strain observed in bending. In the case of hybrid specimens, a decrease in initial stiffness was also observed with ageing but only after 30 days (Figure 7b and Table 2). It was possible that after 10 days of ageing, the composite material in the centre of the specimen was not yet saturated with water because the weight gain was not stabilized for impact specimens after 10 days (Figure 2). As observed in bending specimens, there was no real performance loss between 30 and 177 days, and the absorbed energy even increased. The observations of the impacted specimens (Figure 10b) made it possible to formulate some explanations for this behaviour. For unaged specimens, the area deformed by impact was small, and cracks were present in the skin at the back. With ageing, this area increased significantly due to the more widely distributed plastic deformation in the skins, which were less constrained by the composite core. It is interesting to note that the skins were not cracked during impact after 30 days.

Thermal ageing

To better understand and model the long-term behaviour of such hybrid materials, it is necessary to decouple the effects of water absorption and temperature. Therefore, in this study, thermal ageing was also investigated. For the targeted applications (street furniture and construction), the materials must withstand variable temperatures, which can reach maximum values of approximately 70 °C. The temperature of materials during atmospheric exposure depends on a number of factors related to the material properties but also to the conditions of exposure to solar radiation and the geographical

location. The maximum daily temperature of material under solar radiation was estimated and measured at approximately 75 °C for composite materials [31] and metal [32]. To reproduce long-term ageing (several years or decades) from short trials (several weeks or months), a classical strategy is to accelerate ageing using degradation factors at levels exceeding the service range. This allows the material to reach the same state as a naturally aged material but in a shorter time. The risk in such an approach is, however, to induce mechanisms that do not occur in real ageing. This is almost exactly what has been observed when the hybrid material has been exposed to an accelerated ageing temperature of 120 °C. The adhesive film degraded, and delamination between the stainless steel skins and the composite occurred. This was expected since the melting temperature of the adhesive was approximately 100 °C. The measured shear strength dropped from 4.3 MPa to 0.6 MPa when the temperature was varied from 21 °C to 100 °C using a single-lap shear test. Therefore, the investigation of accelerated thermal ageing was restricted to the scale of the composite material, the component most likely to be altered after the adhesive layer.

Figure 11 shows the evolution of the mass loss as a function of the thermal ageing time. During the first hours, a rapid decrease in mass was observed; afterwards, the mass loss rate slowed over the next days to reach a value of approximately 2.8% after 40 days. This mass loss was attributed to the drying of the sample and, more precisely, to the release of the water remaining in the plant fibres after composite manufacturing. Unexpectedly, after 50 days, a second stage with a significant mass loss was observed with a sharp drop until 120 days, reaching a value of 8.5%. Then the rate of mass loss slowed but remained significant. After 252 days of ageing, a mass loss of approximately 11.5% was finally recorded. This mass loss observed after material dried was attributed

to the degradation of the polypropylene. Indeed, a significant change in colour was observed along with many cracks in the PP matrix of the composite when exposed to thermal ageing (Figure 12). These phenomena were also observed in the neat polymer (Figure 13) and were attributed to the thermal oxidation of polypropylene.

Indeed, in certain circumstances, the thermal oxidation of polypropylene appeared at moderate temperatures (typically below 150 °C) and was heterogeneous at a macroscopic level [33]. This was observed for PP fibres at 110 °C in air at atmospheric pressure [34] and for thin PP films in air at 90 °C [35]. The results showed the presence of predominant chain scission, chemicrystallization and embrittlement. This was attributed to stabilizer consumption. George et al. [36] demonstrated that an infectious spreading kinetic model could simulate the observed behaviour well. The heterogeneous features of the oxidation of polypropylene in the amorphous region were consistent with infectious spreading from a small number of sites, such as catalyst residues. A stochastic model was developed to demonstrate the spatial and temporal development of oxidation at these sites [37].

In the present study, FTIR analyses were performed in the aged materials in the region where degradation was observed (Figures 14 and 15). The region of the FTIR spectrum between 1500 cm^{-1} and 1900 cm^{-1} of the composite aged at 120 °C showed a decrease until a disappearance of the carbonyl band at 1730 cm^{-1} after 50 days. After 252 days of exposure, a broad band with three shoulders at 1775 cm^{-1}, 1730 cm^{-1} and 1715 cm^{-1}, as well as a slight increase in a large band at approximately 1640 cm^{-1}, appeared in the spectrum.

The depletion of the absorption at 1730 cm^{-1} observed during the first 50 days could be attributed to the loss of stabilizer ester groups due to a physical evaporation phenomenon [38, 39]. After 255 days of thermal exposure, the FTIR spectrum of the composite showed a sharp increase in carbonyl functions at 1730 cm^{-1} with the appearance of ketones at 1715 cm^{-1} and peresters or lactones at 1775 cm^{-1} that may have formed during PP degradation [40]. The increase in the absorption at approximately 1640 cm^{-1} revealed a very slight exposure of flax fibres due to a moderate loss of polymer matrix at the composite surface.

From a mechanical point of view, thermal ageing also had significant effects on the composite material. After 10 days of exposure, a slight increase in the bending modulus was measured (Figure 16a and Table 3) that was associated with a significant decrease in stress and strain at failure. This was attributed to the drying of the material. The removal of water molecules led to stiffer but also more brittle behaviour. This effect was exacerbated with ageing time and particularly marked after 252 days. The stress and strain at failure were then divided by factors of 2.6 and 4.6, respectively, when compared to the unaged conditions. This was attributed to the embrittlement of PP due to thermal oxidation and induced fibre/matrix debonding in the infected region.

The impact resistance of the composite was also strongly affected by thermal ageing (Figure 16b and Table 3). The maximum force, energy absorbed and displacement at perforation decreased slightly and progressively for ageing times up to 50 days. This was mainly attributed to the drying of the material. For the bending properties, a significant drop in impact properties was observed after 252 days. The failure mode (Figure 17) was completely different with complete perforation of the plate, without

tearing around the hole. This could again be attributed to the embrittlement of the PP matrix induced by thermal oxidation.

This effect of temperature on this polypropylene-reinforced composite was unexpected. Indeed, thermal oxidation in air for these ranges of exposure times and temperatures has mainly been observed in the literature for fibres and films but not for bulk materials. The question of the effect of flax fibres on PP stabilizers could be raised and deserves to be thoroughly analysed in further studies. Even if quite severe temperatures were applied in this study to accelerate ageing, these temperatures could also be encountered under certain service conditions where they could limit the safe use of such composites over long times.

Conclusion

Studying the durability of FMLs made of PFCs is of primary importance for their safe and reliable introduction in many application sectors, such as outdoor structures. This study investigated the hydrothermal and thermal ageing of a flax/polypropylene composite and its stainless steel hybrid laminates. The results showed that before ageing, the bending stiffness increased by a factor of 6 and the bending strength and impact force by a factor of 3 when the flax/polypropylene composite was hybridized with thin stainless steel sheets. After 177 days of hydrothermal ageing, the remaining bending stiffness and strength in the water-saturated state were approximately 20 GPa and 70 MPa, respectively, and the skins were no longer cracked during impact. The hydrothermal ageing involved reversible mechanisms such as plasticization of flax fibres by water and the activation of viscoelastic properties but also irreversible

mechanisms such as the degradation of interfacial adhesion between steel and composite and between flax fibres and PP and the hydrolysis of flax fibres.

During thermal ageing, the critical points were the shear strength and adhesion between stainless steel sheets and PFC and the thermal oxidation of PP, which induced a drop in the bending and impact properties of flax/PP composites for long exposure times. This was mainly due to the embrittlement of PP attributed to the consumption of PP stabilizers. Loss of stabilizers was also observed during water immersion.

Despite the degradation mechanisms observed for the accelerated ageing protocols used in this study, it was concluded that this new generation of FMLs made of PFCs is suitable for outdoor applications. In real applications, the composite material should be fully protected by stainless steel (including lateral faces) to limit risks of contact between the composite and liquid water, and polypropylene stabilizers suitable with plant fibres also should be used.

Acknowledgments:

The authors acknowledge the Conseil Régional of Bourgogne Franche-Comté (BFC) and the French Agency for Ecological Transition (ADEME) for the granting of a PhD thesis scholarship to N.E. Ngoufo Donkeng. This work has also been supported by the EIPHI Graduate School (contract "ANR-17-EURE-0002").

References:

[1] Sinmazçelik T, Avcu E, Bora MÖ, Çoban O. A review: Fibre metal laminates, background, bonding types and applied test methods. Materials & Design. 2011;32(7):3671-85.

[2] Swolfs Y, Gorbatikh L, Verpoest I. Fibre hybridisation in polymer composites: A review. Composites Part A: Applied Science and Manufacturing. 2014;67:181-200.

[3] Vieira LMG, dos Santos JC, Panzera TH, Rubio JCC, Scarpa F. Novel fibre metal laminate sandwich composite structure with sisal woven core. Industrial Crops and Products. 2017;99:189-95.

[4] Roebroeks GHJJ. Fibre-metal laminates: Recent developments and applications. International Journal of Fatigue. 1994;16(1):33-42.

[5] Vermeeren CAJR. An Historic Overview of the Development of Fibre Metal Laminates. Applied Composite Materials. 2003;10(4):189-205.

[6] Vogelesang LB, Gunnink JW. ARALL: A materials challenge for the next generation of aircraft. Materials & Design. 1986;7(6):287-300.

[7] Reyes V G, Cantwell WJ. The mechanical properties of fibre-metal laminates based on glass fibre reinforced polypropylene. Composites Science and Technology. 2000;60(7):1085-94.

[8] Kuan HTN, Cantwell WJ, Hazizan MA, Santulli C. The fracture properties of environmental-friendly fiber metal laminates. Journal of Reinforced Plastics and Composites. 2011;30(6):499-508.

[9] Ramakrishnan KR, Sarlin E, Kanerva M, Hokka M. Experimental study of adhesively bonded natural fibre composite – steel hybrid laminates. Composites Part C: Open Access. 2021;5:100157.

[10] Santulli C, Kuan HT, Sarasini F, De Rosa IM, Cantwell WJ. Damage characterisation on PP-hemp/aluminium fibre–metal laminates using acoustic emission. Journal of Composite Materials. 2012;47(18):2265-74.

[11] Segovia F, Blanchet P, Amor B, Barbuta C, Beauregard R. Life Cycle Assessment Contribution in the Product Development Process: Case Study of Wood Aluminum-Laminated Panel. Sustainability. 2019;11(8):2258.

[12] Vasumathi M, Murali V. Effect of Alternate Metals for use in Natural Fibre Reinforced Fibre Metal Laminates under Bending, Impact and Axial Loadings. Procedia Engineering. 2013;64:562-70.

[13] Bourmaud A, Beaugrand J, Shah DU, Placet V, Baley C. Towards the design of high-performance plant fibre composites. Progress in Materials Science. 2018;97:347-408.

[14] Liu T, Butaud P, Placet V, Ouisse M. Damping behavior of plant fiber composites: A review. Composite Structures. 2021;275:114392.

[15] Chang BP, Mohanty AK, Misra M. Studies on durability of sustainable biobased composites: a review. RSC Advances. 2020;10(31):17955-99.

[16] Javanshour F, Prapavesis A, Pournoori N, Soares GC, Orell O, Pärnänen T, et al. Impact and fatigue tolerant natural fibre reinforced thermoplastic composites by using non-dry fibres. Composites Part A: Applied Science and Manufacturing. 2022;161:107110.

[17] Lu MM, Van Vuure AW. Improving moisture durability of flax fibre composites by using non-dry fibres. Composites Part A: Applied Science and Manufacturing. 2019;123:301-9.

[18] Lu MM, van Vuure AW. Long-term moisture cycling performance and unexpected strengthening of non-dry flax fibre composites. Industrial Crops and Products. 2023;195:116486.

[19] Huang J, Yves Le Gac P, Richaud E. Thermal oxidation of poly(dicyclopentadiene) - Effect of phenolic and hindered amine stabilizers. Polymer Degradation and Stability. 2021;183:109267.

[20] Panaitescu DM, Vuluga Z, Sanporean CG, Nicolae CA, Gabor AR, Trusca R. High flow polypropylene/SEBS composites reinforced with differently treated hemp fibers for injection molded parts. Composites Part B: Engineering. 2019;174:107062.

[21] El Hachem Z, Célino A, Challita G, Moya M-J, Fréour S. Hygroscopic multi-scale behavior of polypropylene matrix reinforced with flax fibers. Industrial Crops and Products. 2019;140:111634.

[22] Cheng M, Zhong Y, Kureemun U, Cao D, Hu H, Lee HP, et al. Environmental durability of carbon/flax fiber hybrid composites. Composite Structures. 2020;234:111719.

[23] Bourmaud A, Morvan C, Baley C. Importance of fiber preparation to optimize the surface and mechanical properties of unitary flax fiber. Industrial Crops and Products. 2010;32(3):662-7.

[24] Martin N, Mouret N, Davies P, Baley C. Influence of the degree of retting of flax fibers on the tensile properties of single fibers and short fiber/polypropylene composites. Industrial Crops and Products. 2013;49(0):755-67.

[25] Placet V, Day A, Beaugrand J. The influence of unintended field retting on the physicochemical and mechanical properties of industrial hemp bast fibres. Journal of Materials Science. 2017;52(10):5759-77.

[26] Akin DE, Epps HH, Archibald DD, Sharma HSS. Color Measurement of Flax Retted by Various Means. Textile Research Journal. 2000;70(10):852-8.

[27] Guéguen Minerbe M, Durrieu C, Guenne A, Rouillac L, Diafi D, Nour I, et al. Impact of polyethylene and polypropylene geomembranes in sensitive aquatic environment. Ecotoxicology and Environmental Safety. 2018;148:884-91.

[28] Le Duigou A, Bourmaud A, Baley C. In-situ evaluation of flax fibre degradation during water ageing. Industrial Crops and Products. 2015;70:204-10.

[29] Papa I, Formisano A, Lopresto V, Cimino F, Vitiello L, Russo P. Water ageing effects on the mechanical properties of flax fibre fabric/polypropylene composite laminates. Journal of Composite Materials. 2020;54(24):3481-9.

[30] Hamour N, Boukerrou A, Djidjelli H, Maigret J-E, Beaugrand J. Effects of MAPP Compatibilization and Acetylation Treatment Followed by Hydrothermal Aging on Polypropylene Alfa Fiber Composites. International Journal of Polymer Science. 2015;2015:451691.

[31] Tompkins SS, Tenney DR, Unnam J. Prediction of Moisture and Temperature Changes in Composites During Atmospheric Exposure. In: Tsai SW, editor. West Conshohocken, PA: ASTM International; 1979. p. 368-80.

[32] Russell DG, Bartels RA. The temperature of various surfaces exposed to solar radiation: An experiment. The Physics Teacher. 1989;27(3):179-81.

[33] Fayolle B, Audouin L, George GA, Verdu J. Macroscopic heterogeneity in stabilized polypropylene thermal oxidation. Polymer Degradation and Stability. 2002;77(3):515-22.

[34] Fayolle B, Richaud E, Verdu J, Farcas F. Embrittlement of polypropylene fibre during thermal oxidation. Journal of Materials Science. 2008;43(3):1026-32.

[35] Fayolle B, Audouin L, Verdu J. Oxidation induced embrittlement in polypropylene — a tensile testing study. Polymer Degradation and Stability. 2000;70(3):333-40.

[36] G.A. G, M. C. Homogeneous and heterogeneous oxidation of polypropylene. In: Dekker M, editor. Handbook of polymer degradation. New York: CRC Press; 2000.

[37] Goss BGS, Barry MD, Birtwhistle D, George GA. Modelling of infectious spreading in heterogeneous polymer oxidation I. Development of a stochastic model. Polymer Degradation and Stability. 2001;74(2):271-82.

[38] Moisan JY, Lever R. Diffusion des additifs du polyethylene—V: Influence sur le vieillissement du polymère. European Polymer Journal. 1982;18(5):407-11.

[39] Richaud E, Monchy-Leroy C, Colin X, Audouin L, Verdu J. Kinetic modelling of stabilization coupled with stabilizer loss by evaporation. Case of dithioester stabilized polyethylene. Polymer Degradation and Stability. 2009;94(11):2004-14.

[40] Niemczyk A, Dziubek K, Grzymek M, Czaja K. Accelerated laboratory weathering of polypropylene composites filled with synthetic silicon-based compounds. Polymer Degradation and Stability. 2019;161:30-8.

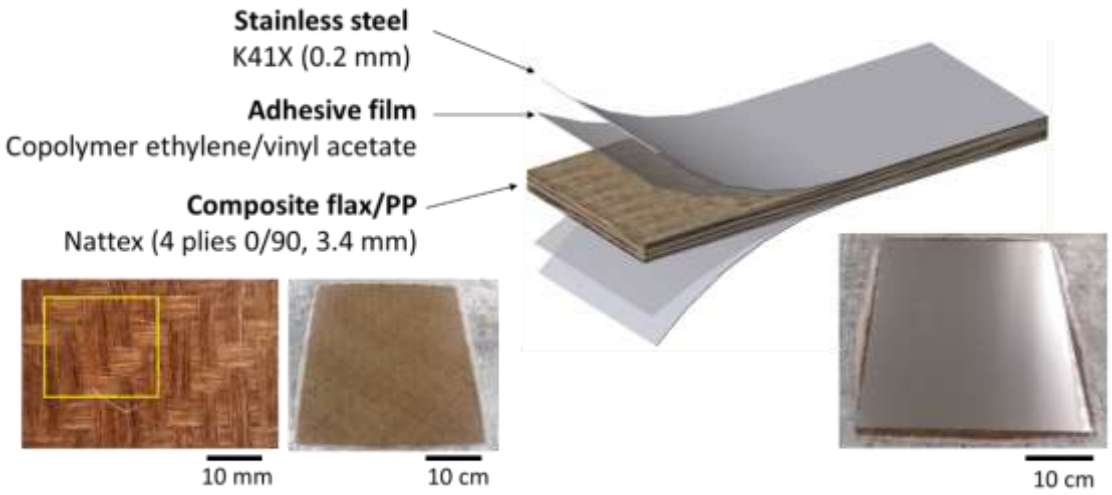

Figure 1: Schematic diagrams and photographs of the hybrid material

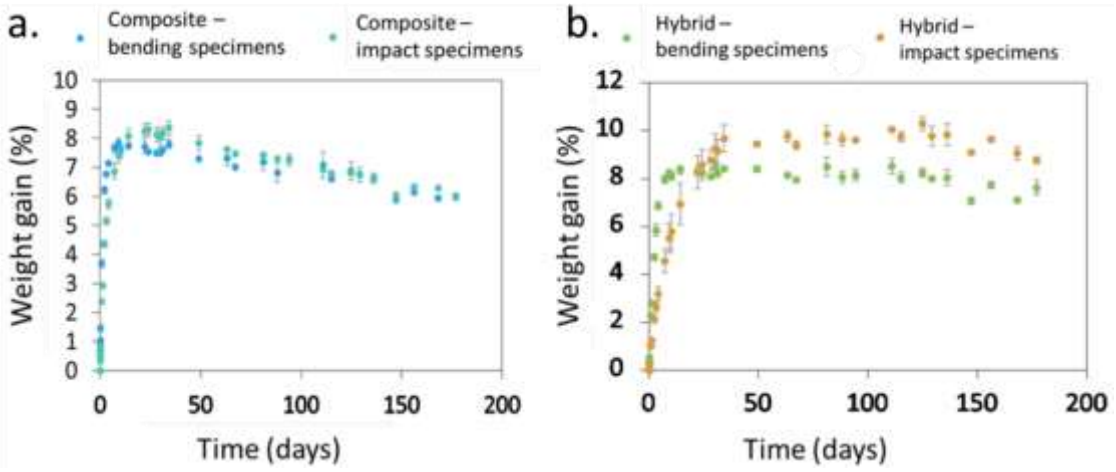

Figure 2: Evolution of the composite (a.) and hybrid (b.) specimen weight as functions of hydrothermal ageing time

Figure 3: Evolution of the appearance of the composite specimens during hydrothermal ageing. a.) Before immersion, b.) immediately after removal from water after 50 days of hydrothermal ageing and c.) after hydrothermal ageing and drying.

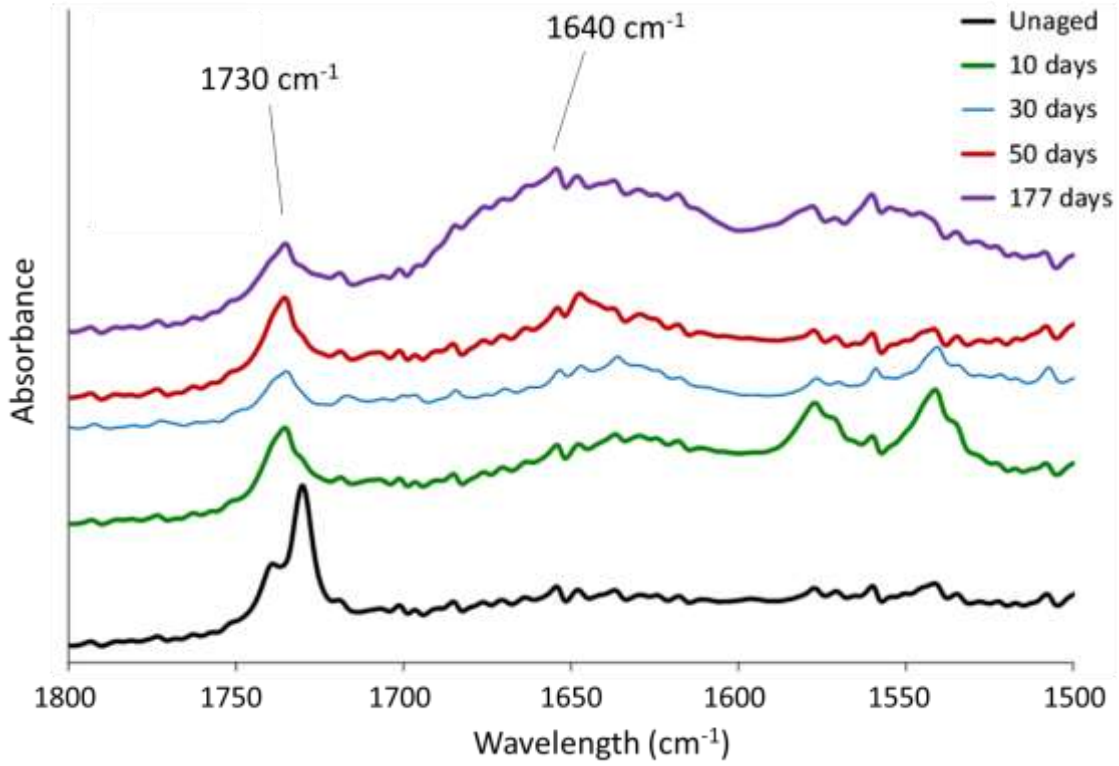

Figure 4: FTIR spectra (vertically shifted for clarity) of the composite during hydrothermal ageing at 70 °C.

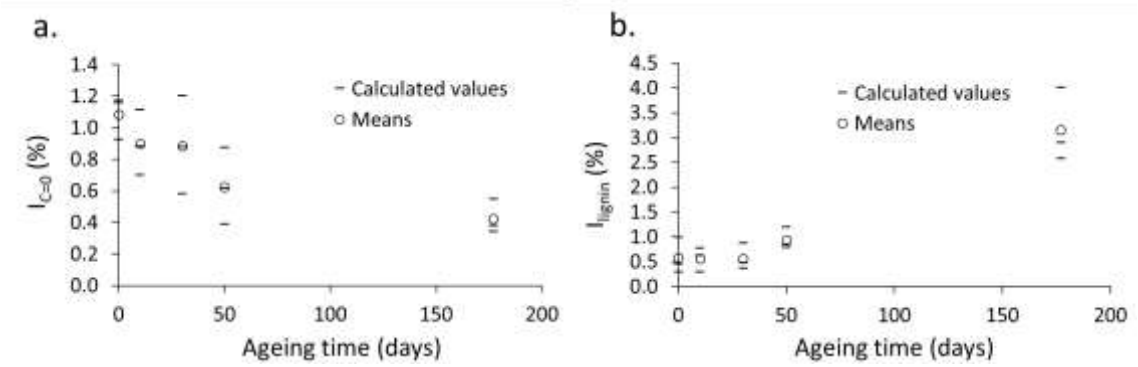

Figure 5: Evolution of the $I_{C=O}$ (a) and I_{lignin} (b) of the composite as functions of exposure time to water at 70 °C according to the alkyl band between 3060 cm^{-1} and 2760 cm^{-1}.

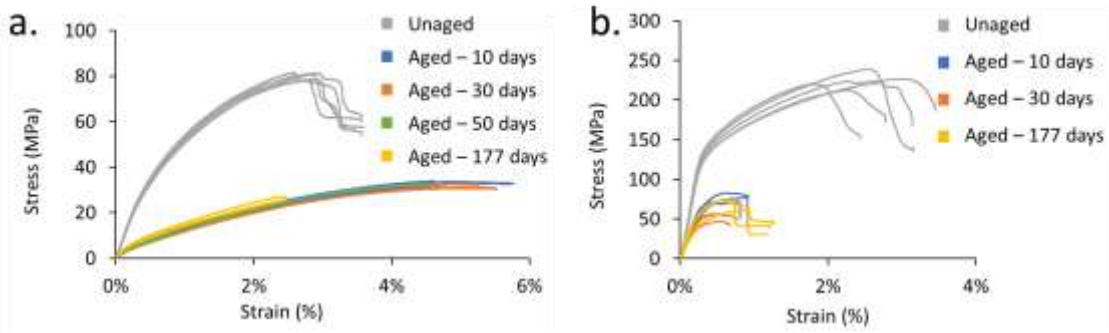

Figure 6: Three-point bending behaviour of composite (a.) and hybrid (b.) materials for different hydrothermal ageing times.

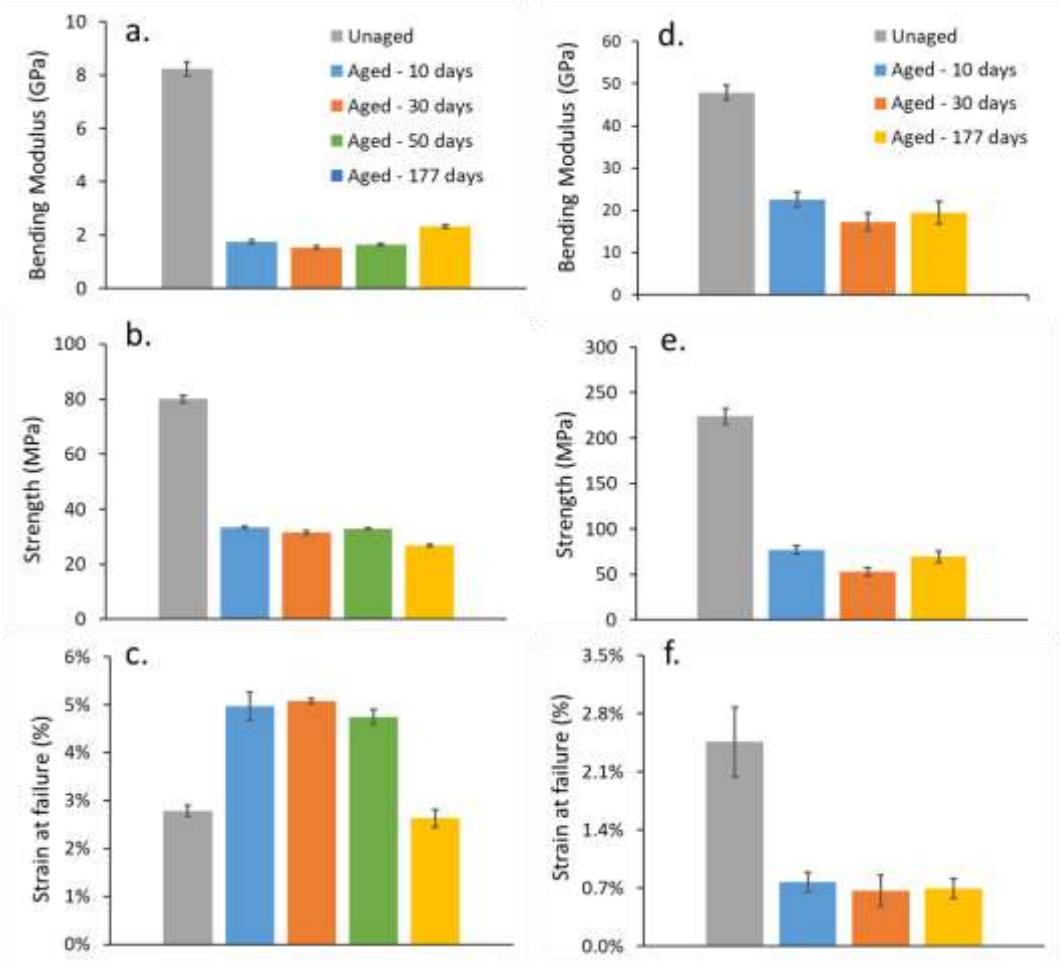

Figure 7: Evolution of the bending modulus, strength and strain at failure for composite (a., b., c., respectively) and hybrid (d., e., f., respectively) materials as functions of the hydrothermal ageing time.

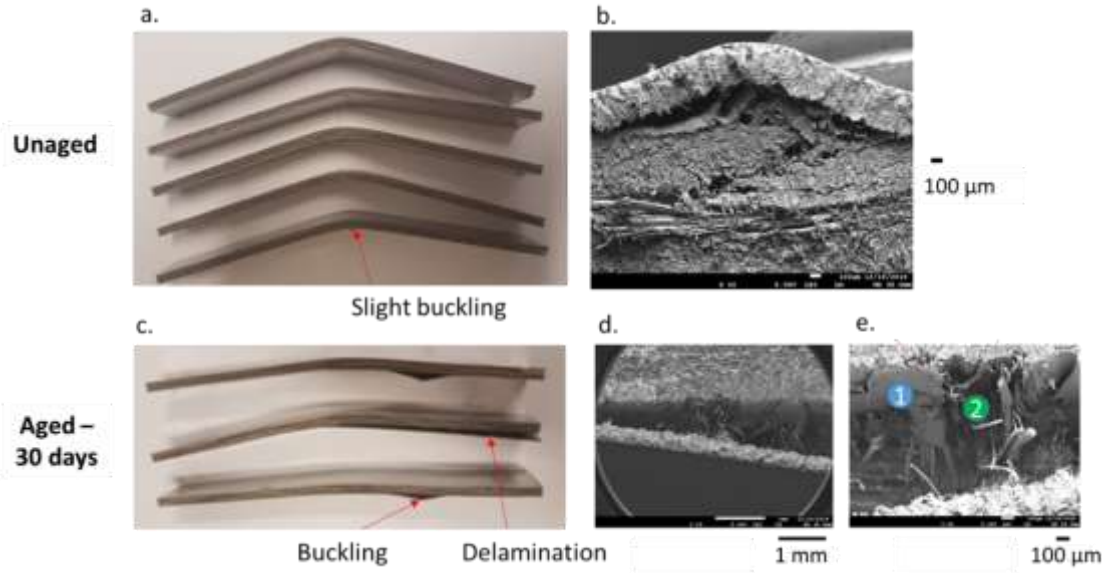

Figure 8: Photographs and scanning electron microscopy observations of hybrid specimens after three-point bending tests before ageing (a. and b.) and after 30 days of hydrothermal ageing (c., d. and e.) Labels 1 and 2 on image e indicate adhesive and cohesive failure zones, respectively.

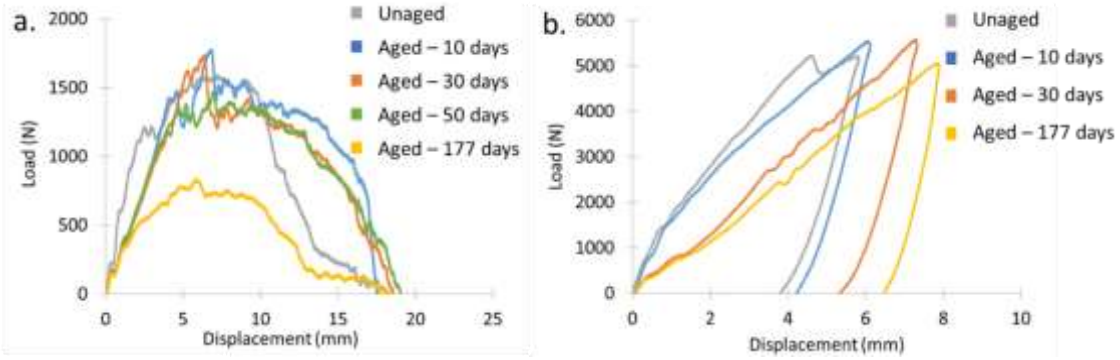

Figure 9: Load vs. displacement curves recorded during impact tests on composite (a.) and hybrid (b.) specimens at different hydrothermal ageing times.

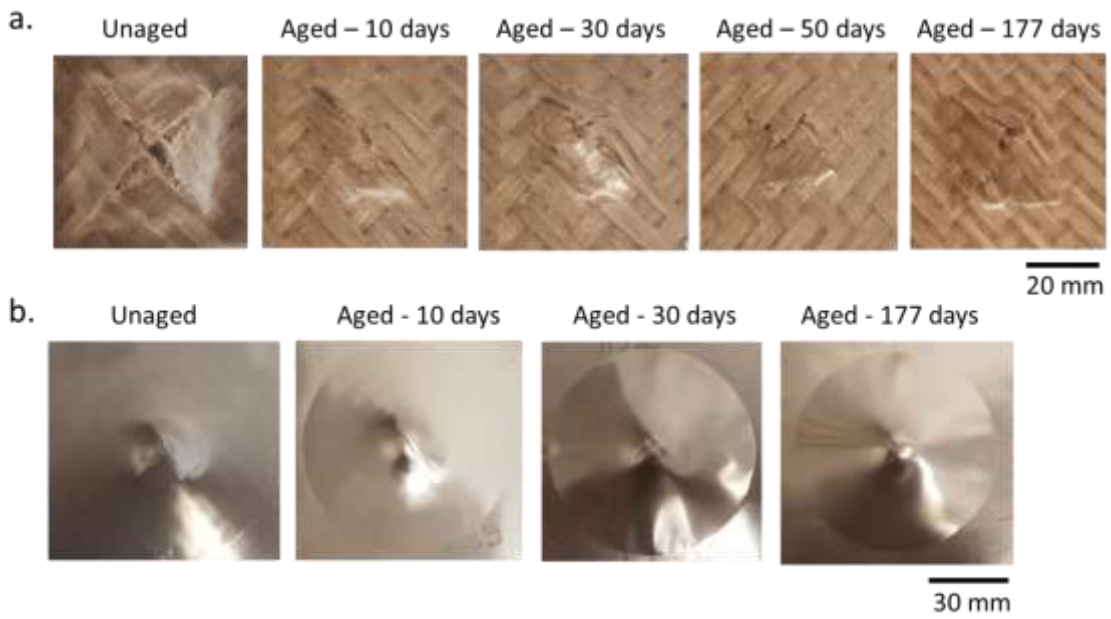

Figure 10: Back surfaces of impacted specimens after different hydrothermal ageing times. (a) composite specimens and (b) hybrid specimens.

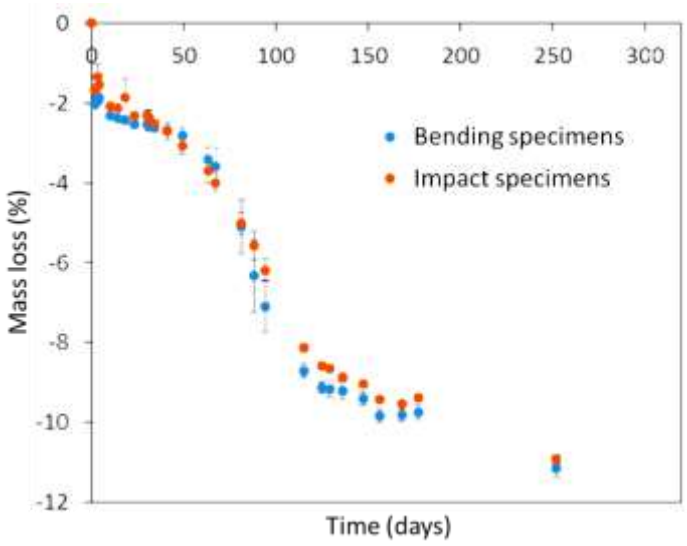

Figure 11: Mass loss as a function of thermal ageing time for composite specimens.

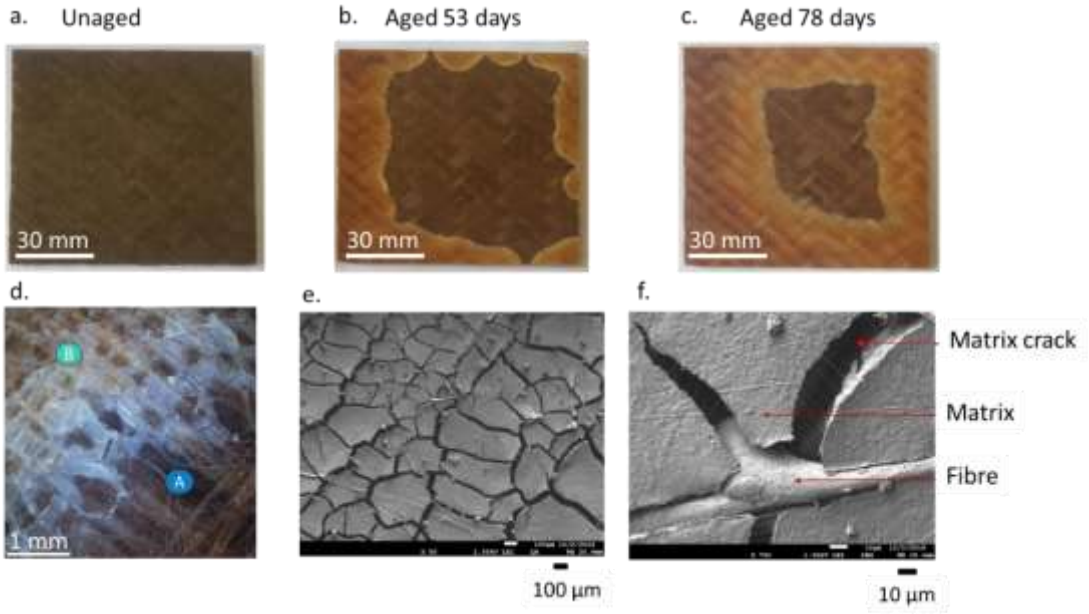

Figure 12: Optical and SEM observations of the composite before and during thermal ageing. Optical images of the composite before ageing (a), after 53 days (b) and 78 days (c) of thermal ageing and magnification of image (c) showing the frontier between the central brown area (label A) and the surrounding yellow zone (label B). SEM images of the aged specimens showing matrix cracks (e) and decohesion at the fibre/matrix interface (f).

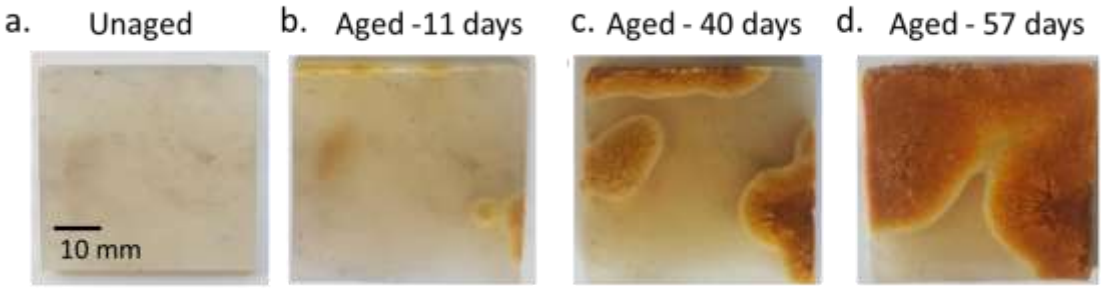

Figure 13: Optical images of polypropylene samples before ageing (a) and after 11 days (b), 40 days (c) and 57 days (d) of thermal ageing.

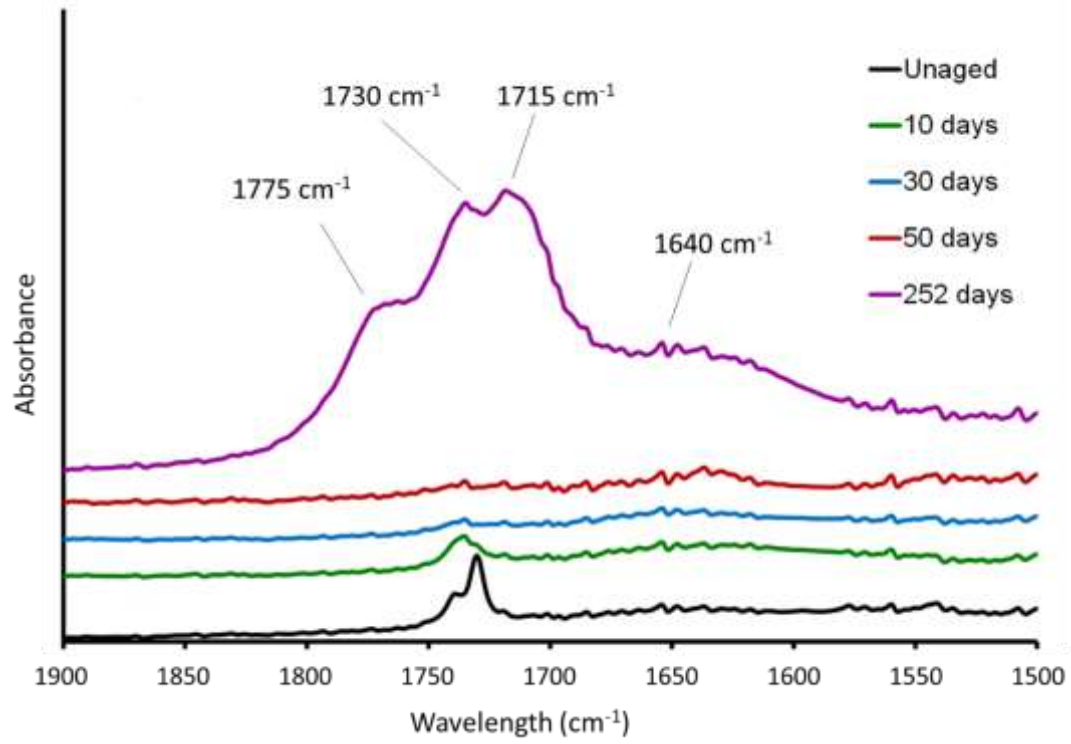

Figure 14: FTIR spectra (vertically shifted for clarity) of the composite under thermal ageing at 120 °C.

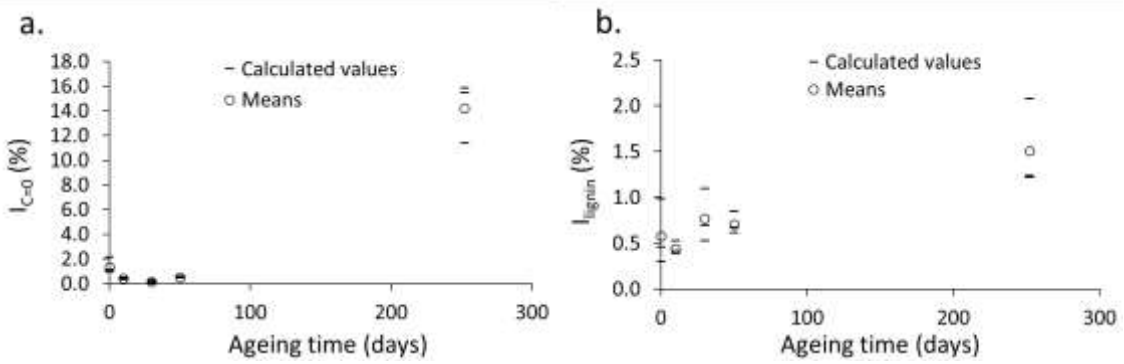

Figure 15: Evolution of the $I_{C=O}$ (a) and I_{lignin} (b) of the composite as functions of the thermal ageing time at 120 °C according to the alkyl band between 3060 cm^{-1} and 2760 cm^{-1}.

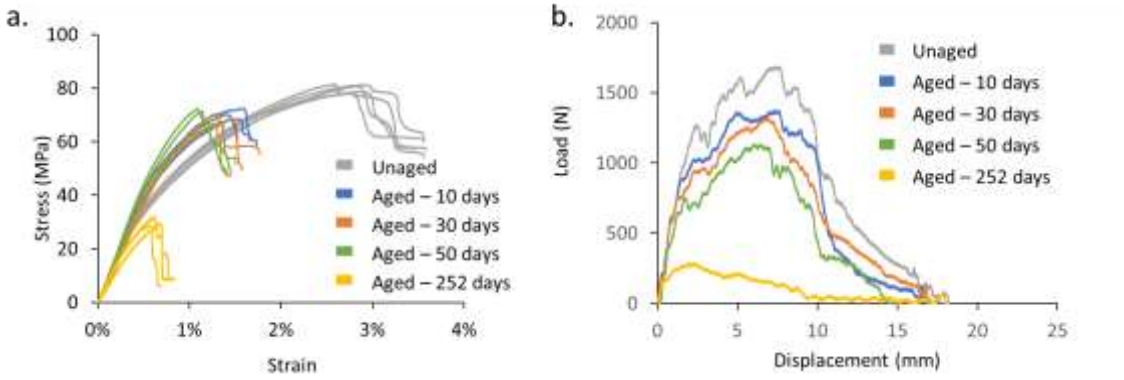

Figure 16: Three-point bending (a) and impact (b) curves recorded for composite specimens at different thermal ageing times.

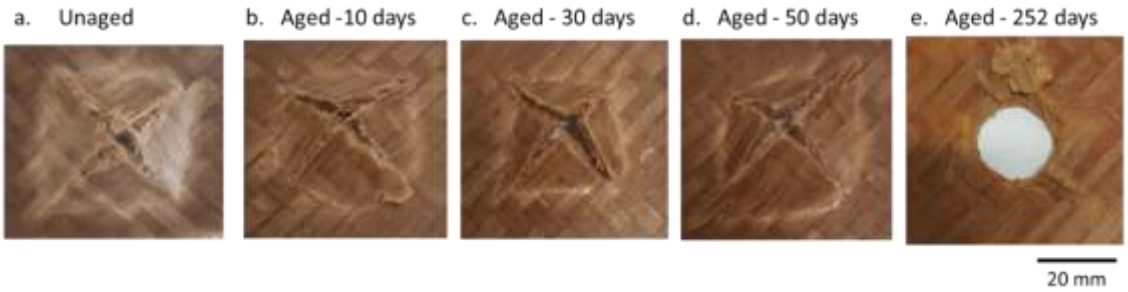

Figure 17: Back surfaces of the composite specimens after impact tests after different thermal ageing times.

Table 1: Mechanical properties of the Nattex composite and the K41X austenitic stainless steel.

	E_1 (GPa)	E_2 (GPa)	ν_{12} (-)	G_{12} (GPa)	G_{13} (GPa)
Nattex	9.3	11.1	0.09	0.85	0.54
	E (GPa)		**ν (-)**	**G (GPa)**	
Stainless steel	220		0.34	82	

Table 2: Impact properties (maximum force, absorbed energy, displacement) for the different tested hydrothermal ageing times (mean values and (standard deviation)).

		Unaged	**10 days**	**30 days**	**50 days**	**177 days**
Composite	Maximum force (N)	1650 (92)	1919 (183)	1789 (47)	1432 (55)	798 (49)
	Energy absorbed at perforation (J)	9.3 (0.7)	6.6 (0.5)	7.1 (1.8)	4.7 (1.4)	3.6 (0.5)
	Displacement at perforation (mm)	7.7 (0.4)	6.7 (0.2)	7.3 (1.6)	5.9 (0.9)	6.7 (0.8)
Hybrid	Maximum force (N)	5270 (172)	5520 (19)	5530 (39)	-	4963 (209)
	Energy absorbed (J)	15.8 (0.3)	16 (0.2)	16 (0.1)	-	17.4 (0.1)
	Maximum displacement (mm)	5.8 (0.1)	6.1 (0.2)	7.4 (0.0)	-	7.9 (0.1)

Table 3: Three-point bending and impact properties of the composite for the different tested thermal ageing times (mean values and (standard deviation)).

		Unaged	10 days	30 days	50 days	252 days
3-point bending	Modulus (GPa)	8.2 (0.3)	8.3 (0.4)	7.7 (0.5)	8.8 (0.4)	6.3 (0.4)
	Strength (MPa)	80.0 (1.4)	70.3 (1.6)	68.2 (1.8)	70.3 (2.1)	30.1 (1.5)
	Strain at failure (%)	2.8 (0.1)	1.5 (0.1)	1.3 (0.1)	1.2 (0.1)	0.6 (0.0)
Impact	Maximum force (N)	1650 (92)	1369 (54)	1313 (14)	1165 (51)	275 (14)
	Energy absorbed at perforation (J)	9.3 (0.7)	7.0 (1.0)	6.0 (0.6)	4.7 (0.2)	0.4 (0.1)
	Displacement at perforation (mm)	7.7 (0.4)	7.0 (0.6)	6.5 (0.5)	5.9 (0.4)	2.2 (0.3)